DOI: 10.1002/ejic.200600995

Synthesis, Characterization, and DFT Investigation of Ir^{III} Tolylterpyridine Complexes

Naokazu Yoshikawa,*[a] Shinichi Yamabe,[b] Nobuko Kanehisa,[c] Yasushi Kai,[c] Hiroshi Takashima,[a] and Keiichi Tsukahara[a]

Keywords: Iridium / Terpyridine / Absorption / Emission / Density functional calculations

Three new polypyridine iridium(III) complexes $[Ir^{III}Cl(L)(tterpy)](PF_6)_2$ {L = phen (**1**), dpphen (**2**), and dmbpy (**3**)} were prepared. Reference complexes $[Ir^{III}Cl(bpy)(tterpy)](PF_6)_2$ (**4**) and $[Ir^{III}(L)_2](PF_6)_3$ {L = tterpy (**5**) and terpy (**6**)} were also prepared. Abbreviations of the ligands used here are phen = 1,10-phenanthroline, dpphen = 4,7-diphenyl-1,10-phenanthroline, bpy = 2,2′-bipyridine, dmbpy = 4,4′-dimethyl-2,2′-bipyridine, tterpy = 4′-(4-tolyl)-2,2′:6′,2′′-terpyridine, and terpy = 2,2′:6′,2′′-terpyridine. The syntheses, which were accomplished in typical reaction times of fifteen minutes by using a microwave oven, were easier than a previous method. The complexes were characterized by electrospray mass spectrometry, UV/Vis spectroscopy, and cyclic voltammetry (CV). The X-ray structures of the two complexes **5** and **6** were also obtained. Cyclic voltammograms of all the $[Ir^{III}Cl(L)(tterpy)]^{2+}$ complexes showed that the first reduction occurred at around –0.67 V, which is attributed to the reduction of the tterpy ligand in $[Ir^{III}Cl(L)(tterpy)]^{2+}$. The electronic properties of complexes **5** and **6** were studied by using B3LYP functional calculations, and their optimized geometries were compared to those of the experimentally observed ones. Excited triplet and singlet states are also examined by using time-dependent density functional theory (TDDFT). The calculated energies of the lowest singlet and triplet states in the two complexes are in good agreement with the experimental absorption and phosphorescence spectra. In this study, it was found that $[Ir^{III}Cl(L)(tterpy)]^{2+}$ emits an intense phosphorescence at room temperature. Since the lowest unoccupied molecular orbitals (LUMOs) of all $[Ir^{III}Cl(L)(tterpy)]^{2+}$ complexes are composed of the π^*-system contribution of the tterpy ligand, the spectroscopic and electrochemical results are discussed comparatively.

Introduction

Polypyridine complexes of d^6 transition metals have been studied extensively because of their useful spectroscopic and photophysical properties. In recent years, much interest has been devoted to Ir^{III} complexes.[1–4] These iridium(III) complexes are known to exhibit high triplet quantum yields due to the mixing of the singlet and triplet excited states through spin-orbital coupling,[5] leading to high phosphorescence efficiencies. The attractive luminescence properties of $[Ir(terpy)_2]^{3+}$, particularly the long lifetime under aerated ambient conditions, render it of interest as the light-emitting component in sensory systems.[6] Bis(terpyridine) complexes of iridium(III) incorporating *meta*- or *para*-*N*-methylpyridyl substituents at the terpyridine 4′ position display long-lived luminescence in solution.[6,7] In particular, Ir^{III} cyclometalated complexes have attracted great attention because of their applications in photonic devices and light-emitting diode (LED) displays.[8,9]

In our previous work, we synthesized and crystallized $[IrCl_2L_2]PF_6$ complexes {L = bqn, phen, dpphen, bpy, and dmbpy} to reveal their long-lived excited states and good photoluminescence efficiencies.[10–13] Abbreviations of the ligands used here are bqn = 2,2′-biquinoline, phen = 1,10-phenanthroline, dpphen = 4,7-diphenyl-1,10-phenanthroline, bpy = 2,2′-bipyridine, and dmbpy = 4,4′-dimethyl-2,2′-bipyridine. Recently, we focused on Ir^{III} complexes with a 2,2′:6′,2′′-terpyridine (terpy) and a polypyridine ligand.[14,15] These iridium complexes have intense phosphorescence at room temperature and remarkably high quantum yields close to unity.[16]

Computational methods were used to predict or confirm photophysical properties of metal complexes. More recently, we designed and synthesized new $[Ru(CH_3CN)(L)(terpy)]^{2+}$ {L = phen, dpbpy, and bpm} complexes, bearing a labile CH_3CN ligand, and their reference complexes $[RuCl(L)(terpy)]^+$ {L = phen, dpbpy, and dpphen}.[17] The time-dependent-density-functional-theory

[a] Department of Chemistry, Faculty of Science, Nara Women's University,
Nara 630-8506, Japan
Fax: +81-742-20-3395
E-mail: naokazuu@dream.com
[b] Department of Chemistry, Nara University of Education, Nara 630-8528, Japan
[c] Department of Applied Chemistry, Graduate School of Engineering, Osaka University,
Osaka 565-0871, Japan
Supporting information for this article is available on the WWW under http://www.eurjic.org or from the author.

(TDDFT) approach provided a good agreement between the computed and the experimental absorption spectra of these ruthenium complexes.[18]

To elucidate the source of intense emission and the electrochemical behavior of the Ir^{III} polypyridine complex and confirm the positions of the HOMO and LUMO in the iridium complexes by using DFT and TDDFT calculations, we tried to synthesize several Ir^{III} complexes with matrixes of a 4′-(4-tolyl)-2,2′:6′,2′′-terpyridine (tterpy) and a polypyridine ligand and also investigate the relations between the structures of a tterpy and a polypyridine ligand and the singlet and triplet electronic states in the iridium complexes. We also report an X-ray crystal structure of $[Ir(tterpy)_2](PF_6)_3$, because crystal structures of Ir^{III}-terpy complexes are very rare.[19,20]

Results and Discussion

X-ray Crystallographic Results

The structural formulae of all the complexes used in this work are shown in Figure 1. The structure of **5**, viz. $[Ir(tterpy)_2](PF_6)_3$, was confirmed by X-ray crystallography (Table 7). The ORTEP view of **5** is shown in Figure 2, and its selected bond lengths and angles are given in Table 1. The crystal structure of a mononuclear iridium compound, **5**, consists of a discrete $[Ir(tterpy)_2]^{3+}$ cation and three hexa-

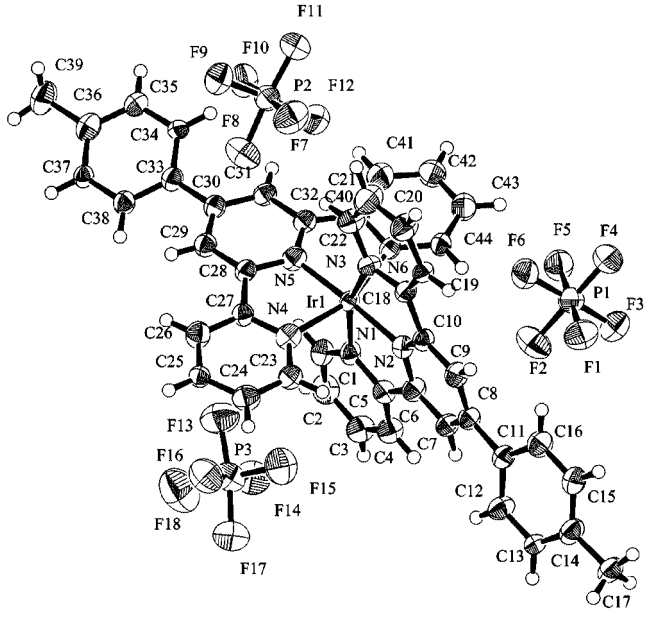

Figure 2. Molecular structure of $[Ir(tterpy)_2](PF_6)_3$ (**5**).

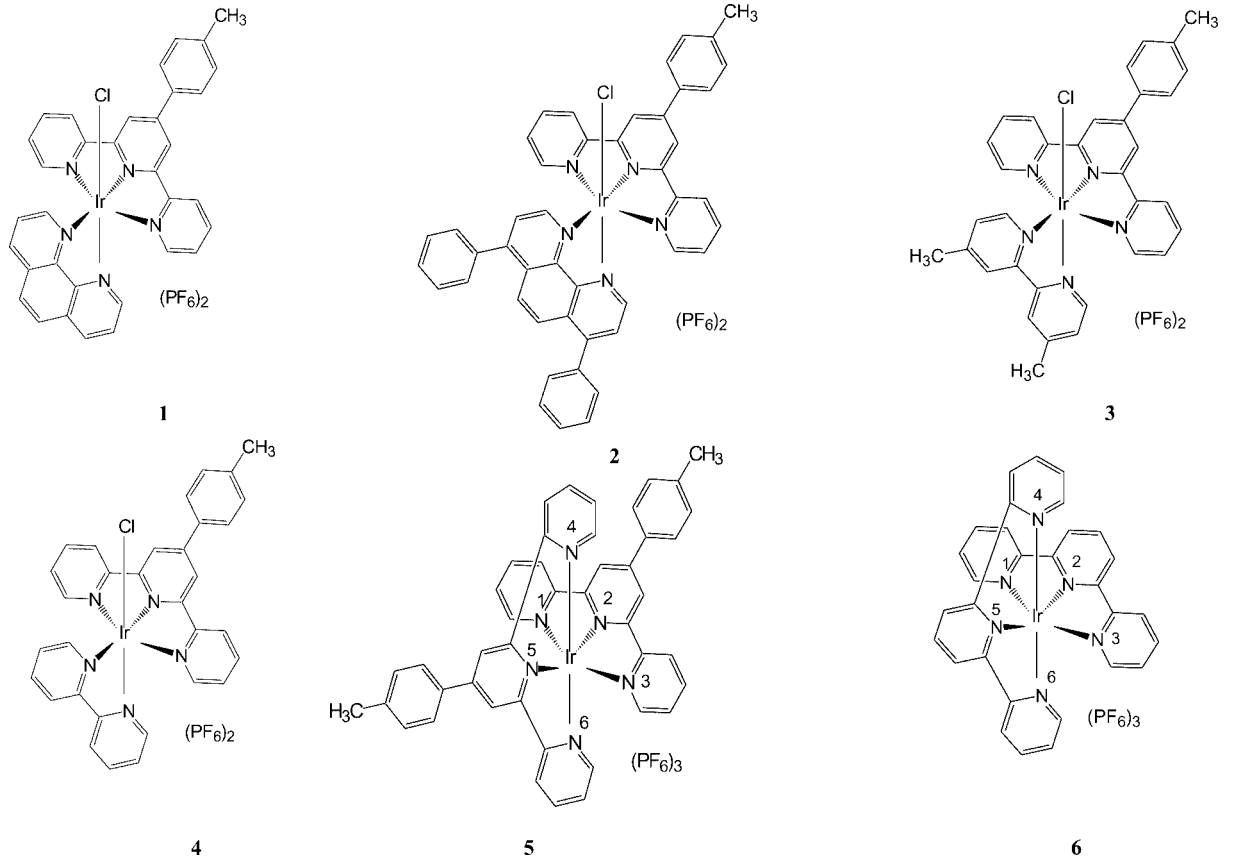

Figure 1. Structural formulae of iridium complexes.

fluorophosphate anions. The Ir^{III} atom is located in a distorted octahedral environment formed by the two tterpy ligands. The Ir–N bond lengths are in the range 1.94(2)–2.09(3) Å and the three *trans* angles are in the range 159.1(7)–176.8(9)°, which are similar to the values of 1.978–2.058 Å and 160.2–177.8° reported for $[Ir(terpy)_2](PF_6)_3$.[19] The Ir cation is coordinated by six N atoms from a pair of chelating tterpy ligands. An equatorial plane is formed by atoms N2, N4, N5, and N6, where the largest deviation from the mean plane is 0.035(4) Å and the Ir atom is out of this plane by 0.013(3) Å. In the case of complex **5**, the axial positions are occupied by the tterpy N1 atom and another tterpy N3 atom. The PF_6^- is not coordinated to the iridium metal atom but hydrogen bonded to ring protons. The average length of the Ir–N bonds is 2.035(2) Å and the average value of the ligand angles, N1–Ir–N2 and N2–Ir–N3 is 79.6(8)°, which compare well with the values of 2.026 Å and 79.1° reported for $[Ir(bpy)_3](ClO_4)_3$.[21]

Table 1. Selected bond lengths and angles for $[Ir(tterpy)_2](PF_6)_3$ (**5**).[a]

Bond length [Å]			Angle [°]		
Ir1–N1	2.04(2)	N1–Ir1–N2	78.5(8)	N3–Ir1–N4	92.3(10)
Ir1–N2	2.02(2)	N1–Ir1–N3	159.1(7)	N3–Ir1–N5	102.2(9)
Ir1–N3	2.09(2)	N1–Ir1–N4	91.2(9)	N3–Ir1–N6	91.1(9)
Ir1–N4	2.09(3)	N1–Ir1–N5	98.7(9)	N4–Ir1–N5	82.0(10)
Ir1–N5	1.94(2)	N1–Ir1–N6	92.6(9)	N4–Ir1–N6	160.2(9)
Ir1–N6	2.03(2)	N2–Ir1–N3	80.7(8)	N5–Ir1–N6	78.2(9)
N7–C45	1.24(4)	N2–Ir1–N4	96.6(9)	N7–C45–C46	167(3)
		N2–Ir1–N5	176.8(9)		
		N2–Ir1–N5	103.3(9)		

[a] Standard deviations are given in parentheses.

Absorption Properties

The electronic absorption spectra for iridium(III) polypyridyl complexes contain typical π–π* and n–π* bands in the ultraviolet region. The electronic absorption spectra for **1**, **2**, and **5** are shown in Figure 3, and the spectroscopic data for the complexes **1**–**6** and the tterpy and terpy ligands are tabulated in Table 2.[22] While the shapes of the spectra are similar, the absorption band at 282 nm for **2** is red shifted relative to that at 272 nm for **1** (Figure 3), owing to the two phenyl groups attached to complex **2**. The absorption band at 272 nm in **1** has been assigned as a phen(π)–phen(π*) transition.[14] Similarly, the bands at 282 nm in **2** could be assigned as dpphen(π)–dpphen(π*) transitions.[10] The absorption bands at 311 nm in both **1** and **2** have been assigned as tterpy(π)–tterpy(π*) transitions. On the other hand, the absorption spectrum of **4** with a bpy ligand is very similar to that of **3** with a dmbpy ligand. This indicates that the two methyl groups introduced in the bpy ligand did not affect the absorption spectra of **3** and **4**. The absorption bands at 252, 278, and 306 nm in the free tterpy are the same as those in **5** (Table 2) and have been assigned as tterpy(π)–tterpy(π*) transitions.[10] Although the free tterpy ligand does not absorb around 320–500 nm, **5** exhibits large absorption bands at 346 and 374 nm. As a consequence of complex formation, the electronic charges are delocalized, and thus the absorption bands at 346 and 306 nm in **5** can be assigned as tterpy(π)–tterpy(π*) transitions. The *para*-tolyl group attached to the terpy ring has the role of expanding the conjugation.

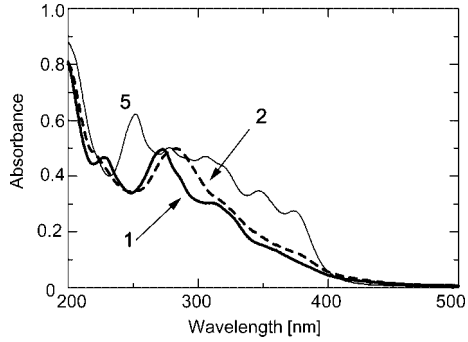

Figure 3. UV spectra of iridium complexes, **1**: $[IrCl(phen)(tterpy)]^{2+}$ (bold line), **2**: $[IrCl(dpphen)(tterpy)]^{2+}$ (broken line), and **5**: $[Ir(tterpy)_2]^{3+}$ (solid line) in CH_3CN solution (1.0×10^{-5} M) at 25 °C.

Electrochemistry

The electrochemical data obtained from cyclic voltammetry (CV) measurements are tabulated in Table 3. As for the complexes **5** and **6**, the first reductions occurred at the same potential (–0.67 V) and were assigned as tterpy/tterpy$^-$ and terpy/terpy$^-$ ligand-centered (LC) processes, respectively.[19] Two successive irreversible reductions of the ligand were then observed as shown in Figure 4. The similarity in

Table 2. Absorption properties for the complexes and ligands in CH_3CN at 25 °C.

	λ_{max} [nm] (ε [10^3 M^{-1} cm^{-1}])					
$[IrCl(phen)(tterpy)](PF_6)_2$ (**1**)		272(49.7)	311(30.2)	359(13.7)		
$[IrCl(dpphen)(tterpy)](PF_6)_2$ (**2**)		282(54.6)	311(37.2)	375(17.3)		
$[IrCl(dmbpy)(tterpy)](PF_6)_2$ (**3**)	253(32.3)	278(30.5)	313(28.3)			
$[IrCl(bpy)(tterpy)](PF_6)_2$ (**4**)	237(34.7)	275(35.0)	313(32.6)			
$[Ir(tterpy)_2](PF_6)_3$ (**5**)	251(62.1)	278(50.3)	306(47.2)	346(34.6)	374(27.8)	
$[Ir(terpy)_2](PF_6)_3$ (**6**)	251(27.6)[a]	277(22.2)[a]	313(11.4)[a]	325(11.8)[a]	352(5.8)[a]	374(1.3)[a]
		273[0.2034][b]	324[0.0794][b]	329[0.1159][b]	348[0.0618][b]	385[0.0113][b]
tterpy	252(43.2)	278(52.0)	306(13.3)			
terpy	237(17.1)	280(15.6)				
	248[0.3289][b]	262[0.1924][b]	275[0.1337][b]	296[0.1569][b]		

[a] Ref.[19] [b] Obtained by RB3LYP/6-31+G*TD calculations. Oscillator strengths are shown in square brackets.

Table 3. Electrochemical properties of the complexes in DMF (V vs. Ag/AgCl).[a]

	E_{1pc}	ΔE_1	E_{2pc}	E_{3pc}	ΔE_3	E_{4pc}	ΔE_4
[IrCl(phen)(tterpy)]$(PF_6)_2$ (**1**)	–0.78		–1.06	–1.27	120	–1.68	130
[IrCl(dpphen)(tterpy)]$(PF_6)_2$ (**2**)	–0.78		–0.99	–1.18	100	–1.63	140
[IrCl(dmbpy)(tterpy)]$(PF_6)_2$ (**3**)	–0.83		–1.06	–1.41	150	–1.70	160
[IrCl(bpy)(tterpy)]$(PF_6)_2$ (**4**)	–0.78		–1.00	–1.27	90	–1.65	100
$[Ir(tterpy)_2](PF_6)_3$ (**5**)	–0.67	70	–0.80				
	–0.81[b]		–0.91[b]				
$[Ir(terpy)_2](PF_6)_3$ (**6**)	–0.67	70	–0.80				
	–0.76[b]		–0.91[b]				

[a] E_{pc} means the reduction peak potential. ΔE is a peak separation between the anodic and cathodic peak potentials. [b] Ref.[19] Potentials are vs. SCE.

these successive reduction potentials between **5** and **6** indicates that both of the reductions occur on the terpyridine ligand frame. Similarly, the first reduction waves of **1** and **2** were at –0.78 V, but the second and third ones appeared at different potentials, –1.06 and –1.27 V for **1** and –0.99 and –1.18 V for **2**. The slightly positive shift in the reduction potential of **2** compared to those in **1** is probably due to the effect of the dpphen ligand (electron-withdrawing ligand). Complexes **3** and **4** gave the second reduction waves at –1.06 and –1.00 V, respectively, as a result of the effect of the electron-donating dmbpy. From these results, both the first and the second reduction waves are assigned as tterpy-centered reductions.[21] Using an electron-donating ligand dmbpy the third reduction potential in **3** was cathodically shifted relative to the reduction potential of **4**, i.e. 140 mV, they can therefore be assigned as polybipyridine-centered reductions. The fourth reduction waves of **1**, **2**, **3**, and **4** occurred at around –1.68, –1.63, –1.70, and –1.65 V, respectively. These processes have also been assigned as tterpy ligand-centered reductions.[10]

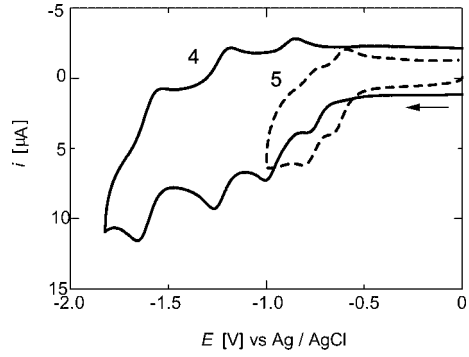

Figure 4. Cyclic voltammograms of **4**: $[IrCl(bpy)(tterpy)]^{2+}$ (bold line) and **5**: $[Ir(tterpy)_2]^{3+}$ (broken line) in CH_3CN solution (5.0×10^{-4} M) at 25 °C with a scan rate of 100 mV s^{-1}.

The typical electrochemical behavior of iridium(III) polypyridine complexes are ligand-site oxidations and reductions. The highest occupied molecular orbital (HOMO) is localized on the ligand molecule, and the oxidative processes take place there. The six 5d lone-pair electrons on Ir^{3+} are not involved in the HOMO, which leads to the absence of MLCT bands in the present six systems. The lowest unoccupied molecular orbital (LUMO) is also localized on the polypyridine ligand. In the case of the iridium complexes comprising a terpy and a bpy ligand, the LUMO is localized on the former ligand.[14]

Emission Properties

The emission maxima and the excited-state lifetimes of the $[IrCl(L)(tterpy)]^{2+}$, $[Ir(tterpy)_2]^{3+}$, and $[Ir(terpy)_2]^{3+}$ systems are given in Table 4. Complex **1** has an intense phosphorescence band maximum at λ_{em} = 537 nm (λ_{ex} = 311 nm) in a solution at room temperature, whereas **2**, having a dpphen ligand, shows a slightly red shifted one at 539 nm (Figure 5). Complex **4** also displays strong phosphorescence at λ_{em} = 542 nm (λ_{ex} = 313 nm), whereas **3** with a dmbpy ligand exhibits a slight blue shift to 535 nm. It was found that the use of dpphen slightly extends the lifetime (τ) of the $^3(\pi^*)$ excited state of the Ir^{III} polypyridine complex (τ = 0.67 μs for **2**). However, in spite of the electron-withdrawing character of dpphen **2** gave a smaller emission quantum yield (ϕ = 0.096) relative to that of **1** (ϕ = 0.165). In complex **3**, the use of the dmbpy instead of the bpy ligand also resulted in the same lifetime as that of the π–π* transition in **3** (τ = 0.68 μs), and its emission quantum yield (ϕ = 0.110) was also similar to that of **4** (ϕ = 0.111). The emission spectrum of complex **5** shows a peak at 506 nm (λ_{ex} = 305 nm) corresponding to the excited state of ^{3}LC whenever the excitation is performed at 270 or 311 nm (Figure 5). This can be assigned to the phosphorescence from the tterpy* excited state (Table 4).[14]

Table 4. Emission properties and lifetimes of the Ir^{III} complexes in CH_3CN at 25 °C.

	λ_{ex} [nm]	λ_{max} [nm]	τ [μs]	ϕ[a]
[IrCl(phen)(tterpy)]$(PF_6)_2$ (**1**)	311	537	0.63	0.165
[IrCl(dpphen)(tterpy)]$(PF_6)_2$ (**2**)	311	539	0.67	0.096
[IrCl(dmbpy)(tterpy)]$(PF_6)_2$ (**3**)	312	535	0.68	0.110
[IrCl(bpy)(tterpy)]$(PF_6)_2$ (**4**)	313	542	0.67	0.111
$[Ir(tterpy)_2](PF_6)_3$ (**5**)	305	506[b]	2.4[b]	0.029[b]
$[Ir(terpy)_2](PF_6)_3$ (**6**)	313	458[b]	1.2, 1.0[b]	0.025[b]

[a] The emission quantum yields were determined for nitrogen-equilibrated samples at 25 °C relative to that of the $[Ru(bpy)_3]^{2+}$ (ϕ = 0.062) solution with the same absorbance. [b] Ref.[19]

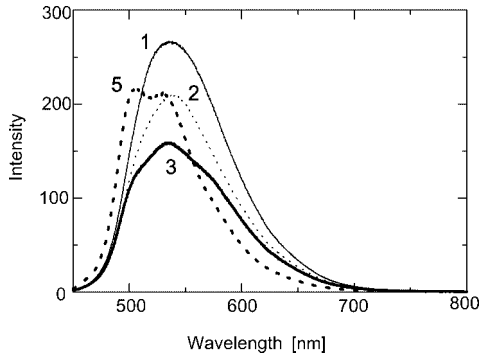

Figure 5. Emission spectra of iridium complexes in degassed CH_3CN solution (1.0×10^{-5} M) at 25 °C. **1**: $[IrCl(phen)(tterpy)]^{2+}$ (bold line), **2**: $[IrCl(dpphen)(tterpy)]^{2+}$ (dotted line), **3**: $[IrCl(dpphen)(tterpy)]^{2+}$ (solid line), and **5**: $[Ir(tterpy)_2]^{2+}$ (broken line).

DFT Calculations and Orbital Analyses

The experimental results obtained here suggest that the frontier orbitals (HOMO and LUMO) of the complexes are composed of the ligand π and π* components. The dπ components do not seem to be involved in the frontier orbitals. The absence of MLCT bands in Ir–terpyridine complexes has also been reported.[14,16] Apparently, the Ir^{3+} cation works as a center of electrostatic stabilization in the complex, in addition to its role in spin-orbit coupling. In order to confirm the trend, DFT calculations were carried out for **5** and **6**. The geometries of $[Ir(tterpy)_2]^{3+}$ and $[Ir(terpy)_2]^{3+}$ were fully optimized in the closed-shell singlet and biradical triplet states. The calculated geometric values in the singlet state are comparable to the experimental ones determined in the present X-ray analyses (Table 5). Calculated metal–ligand bond lengths (angstroms) from singlet and triplet states (parentheses) for iridium complexes are shown in Figure S1. For instance, the calculated values for the Ir–N1 bond length (2.098 Å) and N1–Ir–N2 bond angle (80.2°) of **5** are comparable to the experimental values, 2.04 Å and 78.5°, determined from the X-ray structure, respectively. Calculated spin densities from the triplet state for iridium complexes are given in Figure S2. Table 6 exhibits the thirteen excited states of **6**, which result from low-energy one-electron transitions. The π–π* excitations occur between degenerate atomic orbitals of the tterpy ligand. The HOMO and HOMO–1 should be the frontier donor molecular orbitals, which were found not to be 5dπ but π MOs. The

Table 5. Comparison of the calculated bond lengths and angles from singlet and triplet states for complexes **5** and **6** with the present experimental values from X-ray diffraction.

	Bond length [Å]				Angle [°]		
		Calculated		Experimental		Calculated	Experimental
		Singlet	Triplet	Singlet			
5	Ir–N1	2.098	2.095	2.04(2)	N1–Ir–N2	80.2	78.5(8)
	Ir–N2	2.003	2.010	2.02(2)	N1–Ir–N3	160.3	159.1(7)
	Ir–N3	2.098	2.095	2.09(2)	N1–Ir–N4	91.7	91.2(9)
	Ir–N4	2.098	2.095	2.09(3)	N1–Ir–N5	99.8	98.7(9)
	Ir–N5	2.003	1.985	1.94(2)	N1–Ir–N6	91.6	92.6(9)
	Ir–N6	2.098	2.095	2.03(2)	N2–Ir–N3	80.2	80.7(8)
6	Ir–N1	2.099	2.075	2.054[a]	N1–Ir–N2	80.4	80.3[a]
	Ir–N2	2.006	1.990	1.979[a]	N1–Ir–N3	160.7	160.2[a]
	Ir–N3	2.099	2.075	2.056[a]	N1–Ir–N4	91.6	92.4[a]
	Ir–N4	2.099	2.095	2.058[a]	N1–Ir–N5	99.7	100.4[a]
	Ir–N5	2.006	2.010	1.978[a]	N1–Ir–N6	91.6	91.4[a]
	Ir–N6	2.099	2.095	2.056[a]	N2–Ir–N3	80.4	80.0[a]

[a] From ref.[19]

Table 6. Calculated low-energy excitations in complex **6**.[a]

State	Assignment	*E* [eV]	λ [nm]	*f*
S1	HOMO→LUMO (0.66); HOMO–1→LUMO (0.11); HOMO–2→LUMO (0.17)	3.22	385.34	0.0113
S2	HOMO→LUMO+1 (0.66); HOMO–1→LUMO+1 (0.11); HOMO–2→LUMO+1 (0.17)	3.22	385.33	0.0114
S3	HOMO→LUMO (0.14); HOMO–1→LUMO (0.67)	3.56	348.41	0.0617
S4	HOMO→LUMO+1 (0.14); HOMO–1→LUMO+1 (0.67)	3.56	348.40	0.0618
S5	HOMO→LUMO+2 (0.37); HOMO–3→LUMO+1 (0.33); HOMO–3→LUMO (0.22) HOMO–4→LUMO+1 (0.22); HOMO–4→LUMO (0.33);	3.76	330.01	0.0020
S6	HOMO→LUMO (0.15); HOMO–2→LUMO (0.66)	3.77	328.75	0.1159
S7	HOMO→LUMO+1 (0.15); HOMO–2→LUMO+1 (0.66)	3.77	328.75	0.1159
S8	HOMO→LUMO+2 (0.52); HOMO–1→LUMO+3 (0.23); HOMO–2→LUMO+2 (0.18) HOMO–3→LUMO+1 (0.21); HOMO–3→LUMO (0.14); HOMO–4→LUMO+1 (0.14); HOMO–4→LUMO (0.21);	3.83	323.61	0.0794
S9	HOMO–1→LUMO+3 (0.55); HOMO–2→LUMO+2 (0.39)	4.13	300.46	0.0758
S10	HOMO→LUMO+5 (0.16); HOMO–3→LUMO+3 (0.39); HOMO–4→LUMO+3 (0.24) HOMO–4→LUMO+2 (0.46)	4.16	298.33	0.1173
S11	HOMO→LUMO+6 (0.16); HOMO–3→LUMO+3 (0.24); HOMO–3→LUMO+2 (0.46) HOMO–4→LUMO+3 (0.39)	4.16	298.30	0.1171
S12	HOMO→LUMO+4 (0.13); HOMO→LUMO+2 (0.21); HOMO–1→LUMO+3 (0.27) HOMO–2→LUMO+2 (0.53); HOMO–5→LUMO (0.11); HOMO–6→LUMO+1 (0.11)	4.25	291.62	0.0879
S13	HOMO→LUMO+4 (0.46); HOMO–2→LUMO+4 (0.15); HOMO–5→LUMO+1 (0.19) HOMO–5→LUMO (0.24); HOMO–6→LUMO+1 (0.24); HOMO–6→LUMO (0.20)	4.54	272.93	0.2034

[a] For each singlet state main electron configurations are displayed where absolute values of their coefficients are shown in parentheses.

LUMO, LUMO+1, and LUMO+2 are the expected ligand π* orbitals. Thus, the low-energy one-electron transitions should be mainly HOMO→LUMO, LUMO+1, LUMO+2 and HOMO–1→LUMO, LUMO+1, LUMO+2, which are actually shown in Table 6.

The free terpy and tterpy molecules are nonplanar; the N–C–C–N dihedral angles are 32.1° and 32.02°, respectively. In complexes **5** and **6**, these molecules are fixed to be planar. The forced planarity raises the HOMO energy [–0.246 a.u. (nonplanar) → –0.238 a.u. (planar), by RHF/LANL2MB] and lowers the LUMO energy [+0.194 a.u. (nonplanar) → +0.184 a.u. (planar)]. That is, the forced planarity leads to a smaller HOMO–LUMO energy gap (the larger conjugation) and consequently to a larger λ_{max} value. The question as to why MLCT bands are absent in the $Ir(terpy)_2^{3+}$ complex is considered. In the nearly octahedral geometry of $Ir(terpy)_2^{3+}$ the $5d_{z^2-(x^2+y^2)}$ and $5d_{x^2-y^2}$ atomic orbitals of Ir along the *x*, *y*, and *z* axes are vacant and the $5d_{xy}$, $5d_{yz}$, and $5d_{xz}$ (5dπ orbitals) are lone-pair orbitals. These lone-pair orbitals are low-lying (–1.657 a.u. by RHF/LAN2MB), because the metal center is Ir^{3+}. Scheme 1 illustrates the orbital mixing of the 5dπ-containing occupied MOs. In the Cartesian coordinate shown in Scheme 1, the HOMO of the terpy ring may overlap with the $5d_{xz}$ orbital. The shape of the HOMO is shown in Scheme 2. However, the mixing is very small because the 2pπ coefficient of N3 and N1 is only 0.172 in the terpy HOMO. The HOMO–1 of the terpy ligand may overlap with the $5d_{yz}$ orbital. But the nodal property inside 5dπ orbital again makes the overlap small (Scheme 3). The HOMO–2 cannot overlap with the $5d_{xz}$ (Scheme 4), and the HOMO–3 may overlap with the $5d_{xz}$ orbital. However, the overlap again suffers partial cancellation of Scheme 3. Thus, the MLCT pattern is absent owing to the low orbital energy of Ir^{3+} and the ineffective 5dπ–π orbital overlap.

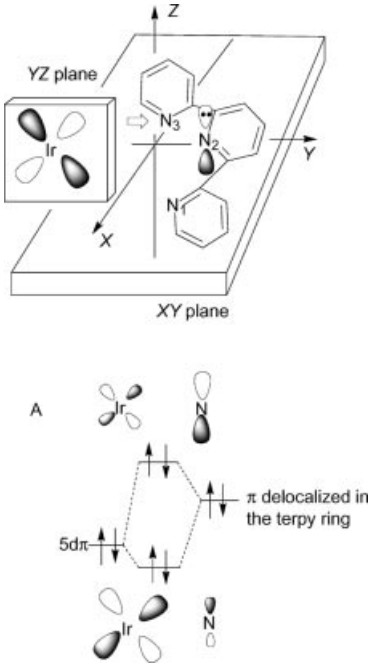

Scheme 1. One example of the orbital mixing that makes high-lying and 5dπ-containing occupied orbitals (A).

Conclusions

Three new polypyridine iridium(III) complexes $[Ir^{II-I}Cl(L)(tterpy)](PF_6)_2$ were prepared {L = phen (**1**), dpphen (**2**), and dmbpy (**3**)}. Reference complexes $[Ir^{III}Cl(bpy)(tterpy)](PF_6)_2$ (**4**) and $[Ir^{III}(L)_2](PF_6)_3$ {L = tterpy (**5**) and terpy (**6**)} were also prepared and the X-ray structure of **5** was obtained. Cyclic voltammograms of all the $[Ir^{III}Cl(L)(tterpy)](PF_6)_2$ complexes showed that the first reduction occurred at around –0.67 V, which is attributed to the reduction of the tterpy ligand in $[Ir^{III}Cl(L)(tterpy)]^{2+}$. The electronic properties of complexes **5** and **6** were studied by using B3LYP functional calculations. Optimized geometries were compared to the experimentally observed structures. Excited singlet and triplet states were examined by using TDDFT. The calculated energies of the lowest singlet state of **6** are in good agreement with experimental absorption spectra. The LUMOs of all $[Ir^{III}Cl(L)(tterpy)]^{2+}$ complexes are composed of the π* system of the tterpy ligand. It was also found that $[Ir^{III}Cl(L)(tterpy)]^{2+}$ emits an intense phosphorescence at room temperature. The spectroscopic and electrochemical results were discussed comparatively. In the DFT calculations for the complexes **5** and **6** these molecules are fixed to be planar. The forced planarity raised the HOMO energy and lowered the LUMO energy, i.e., the forced planarity led to a smaller HOMO–LUMO energy gap (the larger conjugation) and consequently to a larger λ_{max} value. However, the MLCT pattern was absent owing to the low orbital energy of Ir^{3+} and the ineffective 5dπ–π orbital overlap.

Experimental Section

Reagents: The materials used in the present experiments were of analytical reagent grade. The reagents are as follows: ammonium hexachloroiridate {$(NH_4)_3[IrCl_6]$, Aldrich}, bpy (Aldrich), dmbpy (Aldrich), phen (Aldrich), dpphen (Aldrich), tterpy (Aldrich), terpy (Aldrich), and potassium hexafluorophosphate (KPF_6, Wako). Tetrabutylammonium perchlorate {TBAP, $[(C_4H_9)_4N]ClO_4$, Aldrich} as a supporting electrolyte was purchased and used without further purification. CH_3CN and *N*,*N*-dimethylformamide (DMF) used in spectroscopic and electrochemical studies were of spectroscopic grade obtained from Dojindo Laboratory. $[Ir(tterpy)_2](PF_6)_3$ (**5**) and $[Ir(terpy)_2](PF_6)_3$ (**6**) were prepared according to a previous method.[14] All other reagents and solvents were of guaranteed grade.

Syntheses of the Mixed-Ligand Complexes $[IrCl(L)(tterpy)](PF_6)_2$ (1–4): Syntheses of the complexes were undertaken by using a Mitsubishi Electric RR-12AF microwave oven (500 W, 2450 MHz) on medium-high power in a round-bottom flask fitted with a reflux condenser.[10,23] One target complex **3** (L = dmbpy), for example, was prepared by a sequential procedure with a ligand replacement. $(NH_4)_3[IrCl_6]$ (0.238 g, 0.500 mmol) and tterpy (0.161 g, 0.500 mmol) were mixed in ethylene glycol (15 mL). The suspended

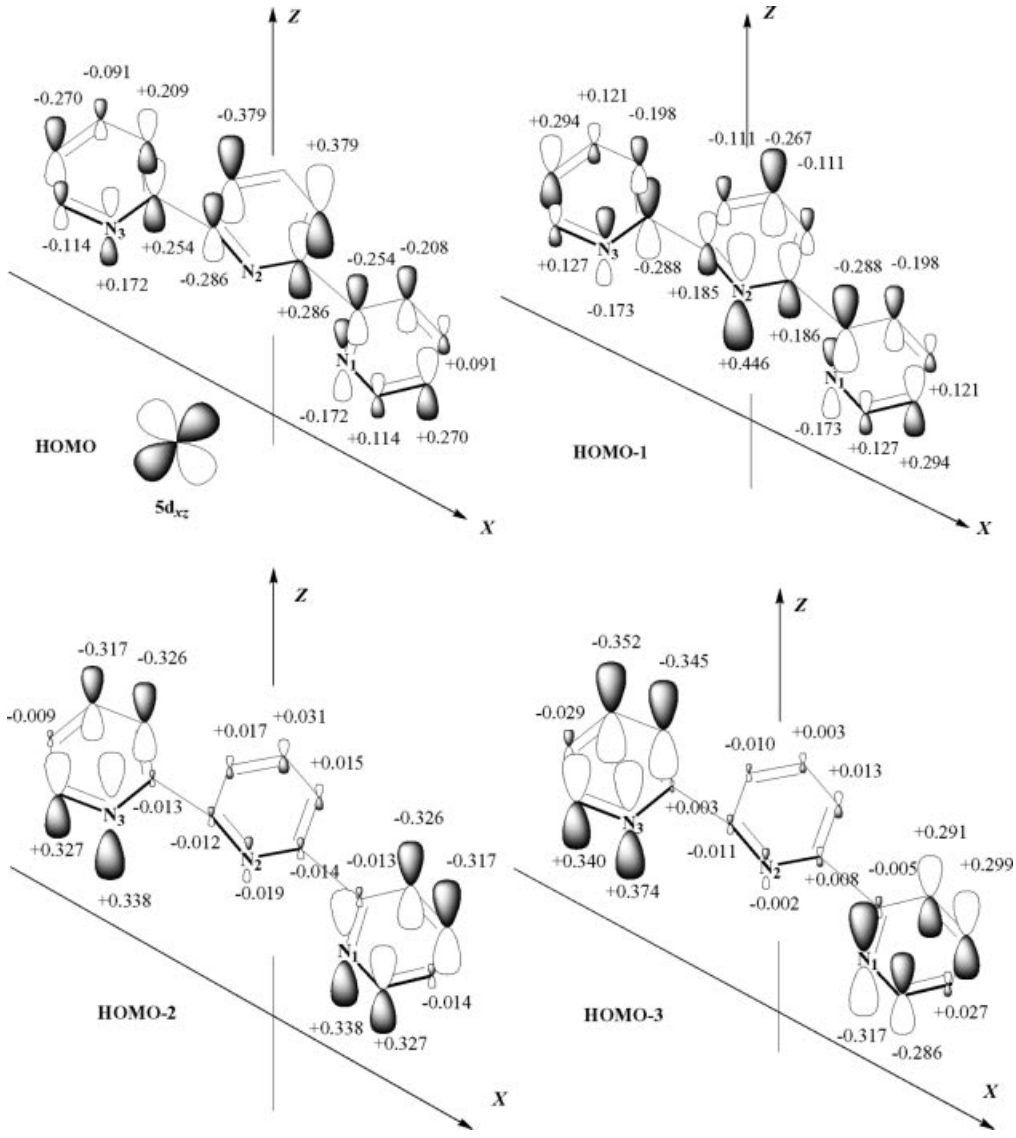

Scheme 2. MOs of the fixed planar terpyridine ligand.

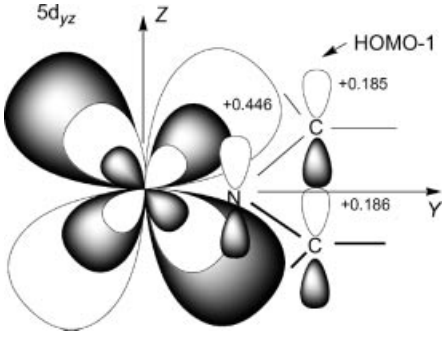

Scheme 3. The overlap between the 5d$_{yz}$ of Ir^{3+} and the HOMO–1 of terpy. The outer white-white overlap in the $Y > 0$, $Z > 0$ region is diminished by the inner shaded-white overlap.

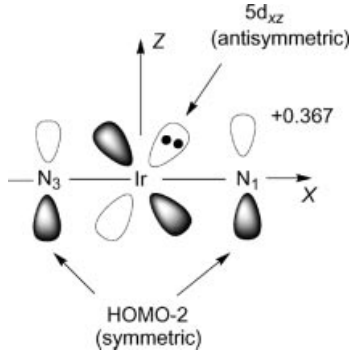

Scheme 4. The overlap between the HOMO–2 and 5d$_{xz}$ is zero (out of phase).

mixture was heated under reflux for 3 min in a microwave oven under a purging nitrogen atmosphere. Next, dmbpy (0.092 g, 0.500 mmol) was added to the mixture, and the refluxing was continued for 12 min. The mixture was then cooled to room temperature. A saturated aqueous solution of KPF_6 (20 mL) was added to provide the counterion PF_6^-, and a light yellow product **3** began to precipitate and was collected by vacuum filtration. The residue was dissolved in a minimal amount of CH_3CN and immediately precipitated in diethyl ether. The product was separated by vacuum filtration and was dried under a vacuum. The purity of the yellow

complex was checked by thin-layer chromatography. Yield: 328 mg (63%). $C_{34}H_{29}ClF_{12}IrN_5P_2{\cdot}H_2O$ (1043.24): calcd. C 39.14, H 3.00, N 6.71; found C 39.47, H 3.15, N 6.30. ^{1}H NMR ([D$_6$]DMSO): δ = 9.50 (s, 1 H, tterpy-H$_{3'}$), 9.31 (s, 1 H, tterpy-H$_{3''}$), 9.13 (d, J = 7.6 Hz, 2 H, tterpy-H), 9.04 (d, J = 8.4 Hz, 1 H, dmbpy-H), 8.87 (s, 1 H, dmbpy-H$_3$) 8.68 (s, 1 H, dmbpy-H$_{3'}$), 8.32 (m, 3 H, tterpy-H, dmbpy-H), 8.23 (d, J = 7.6 Hz, 2 H, tterpy-H), 7.90 (d, J = 7.6 Hz, 2 H, tterpy-H), 7.82 (d, J = 4.8 Hz, 1 H, dmbpy-H), 7.61 (d, J = 8.0 Hz, 1 H, dmbpy-H), 7.57–7.51 (m, 3 H, tterpy-H and tterpy-H), 2.52 (s, 6 H, dmbpy-CH$_3$), 2.04 (s, 3 H, tterpy-CH$_3$) ppm. ESI MS {[IrCl(dmbpy)(tterpy)](PF$_6$)$_2$ in CH$_3$CN, positive}: m/z = 367.51 {[M – (PF$_6$)$_2$]$^{2+}$ requires 367.65}, 879.45 ([M – PF$_6$]$^+$ requires 880.26).

[IrCl(phen)(tterpy)](PF$_6$)$_2$·H$_2$O (1): Yield: 129 mg (22%). $C_{34}H_{25}ClF_{12}IrN_5P_2{\cdot}H_2O$ (1039.23): calcd. C 39.30, H 2.62, N 6.74; found C 39.10, H 2.92, N 6.78. ^{1}H NMR ([D$_6$]DMSO): δ = 9.97 (d, J = 5.2 Hz, 1 H, phen-H), 9.92 (d, J = 5.2 Hz, 1 H, tterpy-H), 9.50 (s, 1 H, tterpy-H), 9.36 (s, 1 H, tterpy-H), 9.26 (dd, J = 8.0 Hz, 1 H, phen-H), 9.13 (t, J = 8.4 Hz, 1 H, tterpy-H), 9.05 (d, J = 8.0 Hz, 1 H, tterpy-H), 8.78 (d, J = 8.0 Hz, 1 H, phen-H), 8.72 (d, J = 8.0 Hz, 1 H, tterpy-H), 8.56 (d, J = 8.4 Hz, 1 H, phen-H), 8.46 (d, J = 5.6 Hz, 1 H, tterpy-H), 8.35–8.26 (m, 3 H, phen-H, tterpy-H and tterpy-H), 8.04 (d, J = 5.2 Hz, 1 H, tterpy-H), 7.91 (d, J = 6.4 Hz, 1 H, phen-H), 7.74 (dd, J = 5.2 Hz, 1 H, phen-H), 7.67–7.61 (m, 2 H, tterpy-H and tterpy-H), 7.58–7.48 (m, 3 H, phen-H, tterpy-H, and tterpy-H), 2.03 (s, 3 H, tterpy-CH$_3$) ppm. ESI MS {[IrCl(phen)(tterpy)](PF$_6$)$_2$ in CH$_3$CN, positive}: m/z = 365.52 {[M – (PF$_6$)$_2$]$^{2+}$ requires 365.64}, 875.47 ([M – PF$_6$]$^+$ requires 876.25).

[IrCl(dpphen)(tterpy)](PF$_6$)$_2$·2H$_2$O (2): Yield: 108 mg (18%). $C_{46}H_{33}ClF_{12}IrN_5P_2{\cdot}2H_2O$ (1209.44): calcd. C 45.68, H 3.08, N 5.79; found C 45.94, H 3.46, N 5.59. ^{1}H NMR ([D$_6$]DMSO): δ = 10.08 (dd, J = 5.6 Hz, 1 H, dpphen-H), 9.45 (s, 1 H, tterpy-H), 9.37 (s, 1 H, tterpy-H), 9.19 (d, J = 8.4 Hz, 1 H), 9.14 (d, J = 8.4 Hz, 2 H, tterpy-H), 8.60 (d, J = 5.6 Hz, 1 H, dpphen-H), 8.52 (d, J = 5.6 Hz, 1 H), 8.48 (d, J = 8.0 Hz, 1 H), 8.43–8.27 (m, 3 H, tterpy-H), 8.22 (d, J = 9.2 Hz, 1 H), 7.93 (d, J = 6.0 Hz, 1 H), 7.89 (dd, J = 8.0 Hz, 2 H), 7.84–7.71 (m, 5 H, tterpy-H), 7.69–7.55 (m, 8 H, tterpy-H), 2.06 (s, 3 H, tterpy-CH$_3$) ppm. ESI MS {[IrCl(dpphen)(tterpy)](PF$_6$)$_2$ in CH$_3$CN, positive}: m/z = 441.46 {[M – (PF$_6$)$_2$]$^{2+}$ requires 441.74}.

[IrCl(bpy)(tterpy)](PF$_6$)$_2$·H$_2$O (4): Yield: 249 mg (48%). $C_{32}H_{25}ClF_{12}IrN_5P_2{\cdot}H_2O$ (1015.20): calcd. C 37.86, H 2.68, N 6.90; found C 38.34, H 3.09, N 6.60. ^{1}H NMR ([D$_6$]DMSO): δ = 9.73 (d, J = 4.8 Hz, 1 H, bpy-H), 9.33 (s, 2 H, tterpy-H), 9.05 (d, J = 8.0 Hz, 2 H, tterpy-H), 9.00 (d, J = 7.2 Hz, 1 H, bpy-H), 8.80 (d, J = 8.0 Hz, 1 H, bpy-H), 8.65 (t, J = 8.0 Hz, 1 H, bpy-H), 8.32 (dd, J = 7.6 Hz, 2 H, tterpy-H), 8.25–8.22 (m, J = 8.8 Hz, 3 H, tterpy-H and bpy-H), 8.17 (t, J = 7.2 Hz, 1 H, bpy-H), 7.97 (d, J = 5.2 Hz, 1 H, bpy-H), 7.83 (d, J = 5.6 Hz, 2 H, tterpy-H), 7.63 (t, J = 6.4 Hz, 2 H, tterpy-H), 7.56 (d, J = 8.0 Hz, 2 H, tterpy-H), 7.42 (t, J = 7.2 Hz, 1 H, bpy-H), 2.52 (s, 3 H, tterpy-CH$_3$) ppm. ESI MS {[IrCl(bpy)(tterpy)](PF$_6$)$_2$ in CH$_3$CN, positive}: m/z = 353.53 {[M – (PF$_6$)$_2$]$^{2+}$ requires 353.62}, 851.51 ([M – PF$_6$]$^+$ requires 852.22).

Measurements: Electronic absorption spectra were recorded at room temperature in CH$_3$CN solution with a Shimadzu UV-2550 spectrophotometer. ESI-MS spectra were obtained by an Applied Biosystems Mariner spectrometer. All NMR spectra were recorded with a JEOL JNM-AL400 FT spectrometer. ^{1}H NMR chemical shift values are reported in ppm with reference to the internal standard TMS. Cyclic voltammograms were measured with an ALS-610B electrochemical analyzer fitted with a three-electrode system consisting of a glassy carbon working electrode, a platinum auxiliary electrode, and a Ag/AgCl reference electrode (0.21 V vs. NHE at 3.5 M KCl). CV experiments were performed on DMF solution of the complexes (5.0×10^{-4} M) and 0.050 M TBAP under nitrogen at 25 °C with a scan rate of 100 mV s^{-1}. The emission lifetimes were measured in nitrogen-equilibrated CH$_3$CN solutions using a Horiba single-photon counting system (NAES-500). The emission quantum yields for the iridium complexes were determined in CH$_3$CN at room temperature relative to those of a solution containing [Ru(bpy)$_3$]$^{2+}$ and having the same absorbance. The emission quantum yields for the iridium complexes were determined by comparing the integrated emission spectra and using ϕ = 0.062 for the standard.[24]

Crystallographic Data Collection and Structure Determination of 5: Crystals for the X-ray diffraction study were mounted on glass fibers. All of the measurements were made with a Rigaku R-Axis-Rapid Imaging Plate diffractometer with graphite monochromated Mo-K_α radiation (see Table 7).[25] Indexing was performed from three oscillations. The camera radius was 127.40 mm. Readout was performed in the 0.100 mm pixel mode. The structures were solved by direct methods and were refined on F^2 by full-matrix least-squares methods using SHELXL-97.[26] The non-hydrogen atoms were refined anisotropically by the full-matrix least-squares method. All hydrogen atoms were anisotropically refined. CCDC-619118 contains the supplementary crystallographic data for this paper. These data can be obtained free of charge from The Cambridge Crystallographic Data Centre via www.ccdc.cam.ac.uk/data_request/cif.

Table 7. Crystallographic data of the iridium complex.

Empirical formula	$C_{48}H_{40}F_{18}IrN_8P_3$ (**5**)
Formula mass [g mol^{-1}]	1356.01
Crystal system	monoclinic
Space group	*Cc*
a [Å]	14.7995(5)
b [Å]	16.4658(5)
c [Å]	21.5521(7)
β [°]	105.5450(8)
Z	4
λ(Mo-K_α) [Å]	0.71073
R_{int}	0.101
θ_{max}	30.5
h	–21 to 21
k	–23 to 22
l	–30 to 30
Total reflections	27453
Unique reflections	7614
μ [mm^{-1}]	2.852
D_c [Mg m^{-3}]	1.780
T [K]	296
V [Å^3]	5059.8(3)
R_1	0.060
R_w	0.140
S	1.19

Computational Methods: DFT calculations of **5** and **6** were performed using the Gaussian 98 program package.[27] The Becke three parameters hybrid exchange and the Lee–Yang–Parr correlation functionals (B3LYP) were used.[28,29] Geometries of **5** and **6** in the singlet closed-shell and triplet biradical states were optimized by the R(U)B3LYP/LANL2MB method.[30] Absorption spectra were computed as vertical excitations from the S_0 PES using the TDDFT approach as implemented in the Gaussian 98 program. A double-ξ quality LANL2DZ basis was used for the iridium atom,[31] and

the other atoms were described by a split valence Pople basis plus one polarization and one diffuse function (6-31+G*).[32]

Supporting Information (see footnote on the first page of this article): A PDF file containing calculated parameters for the iridium complexes (**3**, **5**, and **6**).

[1] E. Baranoff, J.-P. Collin, J.-P. Sauvage, L. Flamigni, *Chem. Soc. Rev.* **2004**, *33*, 147.
[2] A. J. Wilkinson, A. E. Goeta, C. E. Foster, J. A. G. Williams, *Inorg. Chem.* **2004**, *43*, 6513.
[3] K. Dedeian, J. Shi, N. Shepherd, E. Forsythe, D. C. Morton, *Inorg. Chem.* **2005**, *44*, 4445.
[4] L. Flamigni, B. Venture, F. Barigelletti, E. Baranoff, J.-P. Collin, J.-P. Sauvage, *Eur. J. Inorg. Chem.* **2005**, 1312.
[5] A. B. Tamayo, B. D. Alleyne, P. I. Djurovich, S. Lamansky, I. Tsyba, N. H. Ho, R. Bau, E. Thompson, *J. Am. Chem. Soc.* **2003**, *125*, 7377.
[6] K. J. Arm, W. Leslie, J. A. G. Williams, *Inorg. Chim. Acta* **2006**, *359*, 1222.
[7] W. Goodall, J. A. G. Williams, *J. Chem. Soc., Dalton Trans.* **1985**, *82*, 299.
[8] S. Lamansky, P. Djurovich, D. Murphy, F. Abdel-Razzaq, H. E. Lee, C. Adachi, P. E. Burrows, S. R. Forrest, M. E. Thompson, *J. Am. Chem. Soc.* **2001**, *123*, 4304.
[9] M. K. Nazeeruddin, R. Humphry-Baker, D. Bemer, S. Rivier, L. Zuppiroll, M. Graetzel, *J. Am. Chem. Soc.* **2003**, *125*, 8790.
[10] N. Yoshikawa, J. Sakamoto, T. Matsumura-Inoue, H. Takashima, K. Tsukahara, N. Kanehisa, Y. Kai, *Anal. Sci.* **2004**, *20*, 711.
[11] N. Yoshikawa, J. Sakamoto, N. Kanehisa, Y. Kai, T. Matsumura-Inoue, H. Takashima, K. Tsukahara, *Acta Crystallogr., Sect. E* **2003**, *59*, m155.
[12] N. Yoshikawa, J. Sakamoto, N. Kanehisa, Y. Kai, T. Matsumura, H. Takashima, K. Tsukahara, *Acta Crystallogr., Sect. E* **2003**, *59*, m551.
[13] N. Yoshikawa, J. Sakamoto, N. Kanehisa, Y. Kai, T. Matsumura-Inoue, H. Takashima, K. Tsukahara, *Acta Crystallogr., Sect. E* **2003**, *59*, m972.
[14] N. Yoshikawa, T. Matsumura-Inoue, *Anal. Sci.* **2003**, *19*, 761.
[15] N. Yoshikawa, J. Sakamoto, N. Kanehisa, Y. Kai, T. Matsumura-Inoue, H. Takashima, K. Tsukahara, *Acta Crystallogr., Sect. E* **2003**, *59*, m832.
[16] T. Yutaka, S. Obara, S. Ogawa, K. Nozaki, N. Ikeda, T. Ohno, Y. Ishii, K. Sakai, M. Haga, *Inorg. Chem.* **2005**, *44*, 4737.
[17] N. Yoshikawa, S. Yamabe, N. Kanehisa, Y. Kai, H. Takashima, K. Tsukahara, *Inorg. Chim. Acta* **2006**, *359*, 4585.
[18] C. Yang, S. Li, Y. Chi, Y. Cheng, Y. Yeh, P. Chou, G. Lee, C. Wang, C. Shu, *Inorg. Chem.* **2005**, *44*, 7770.
[19] J.-P. Collin, I. M. Dixon, J.-P. Sauvage, J. A. G. Williams, F. Barigelletti, L. Flamigni, *J. Am. Chem. Soc.* **1999**, *121*, 5009.
[20] K. K.-W. Lo, C.-K. Chung, D. C.-M. Ng, N. Zhu, *New J. Chem.* **2002**, *26*, 81.
[21] A. C. Hazell, *Acta Crystallogr., Sect. C* **1984**, *40*, 806.
[22] N. P. Ayala, C. M. Flynn Jr, L. A. Sacksteder, J. N. Demas, B. A. DeGraff, *J. Am. Chem. Soc.* **1990**, *112*, 3837.
[23] P. A. Anderson, L. F. Anderson, M. Furue, P. C. Junk, F. R. Keene, B. T. Patterson, B. D. Yeomans, *Inorg. Chem.* **2000**, *39*, 2721.
[24] J. V. Casper, T. J. Meyer, *Inorg. Chem.* **1983**, *22*, 2444.
[25] N. Yoshikawa, A. Ichimura, N. Kanehisa, Y. Kai, H. Takashima, K. Tsukahara, *Acta Crystallogr., Sect. E* **2005**, *61*, m55.
[26] G. M. Sheldrick, *SHELXL 97*, University of Göttingen, Germany, **1997**.
[27] M. J. Frisch, G. W. Trucks, H. B. Schlegel, G. E. Scuseria, M. A. Robb, J. R. Cheeseman, V. G. Zakrzewski, J. A. Montgomery Jr, R. E. Stratmann, J. C. Burant, S. Dapprich, J. M. Millam, A. D. Daniels, K. N. Kudin, M. C. Strain, O. Farkas, J. Tomasi, V. Barone, M. Cossi, R. Cammi, B. Mennucci, C. Pomelli, C. Adamo, S. Clifford, J. Ochterski, G. A. Petersson, P. Y. Ayala, Q. Cui, K. Morokuma, D. K. Malick, A. D. Rabuck, K. Raghavachari, J. B. Foresman, J. Cioslowski, J. V. Ortiz, A. G. Baboul, B. B. Stefanov, G. Liu, A. Liashenko, P. Piskorz, I. Komaromi, R. Gomperts, R. L. Martin, D. J. Fox, T. Keith, M. A. Al-Laham, C. Y. Peng, A. Nanayakkara, C. Gonzalez, M. Challacombe, P. M. W. Gill, B. Johnson, W. Chen, M. W. Wong, J. L. Andres, C. Gonzalez, M. Head-Gordon, E. S. Replogle, J. A. Pople, *GAUSSIAN 98, Revision A.7*, Gaussian Inc., Pittsburgh PA, USA, **1998**.
[28] C. Lee, W. Yang, R. G. Parr, *Phys. Rev. B* **1988**, *37*, 785.
[29] A. D. Becke, *J. Chem. Phys.* **1993**, *98*, 5648.
[30] J. Hay, W. R. Wadt, *J. Chem. Phys.* **1985**, *82*, 299.
[31] T. H. Dunning Jr, P. J. Hay, *Modern Theoretical Chemistry* (Ed.: H. F. Schaefer III), Plenum, New York, **1976**, p. 1.
[32] M. M. Francl, W. J. Petro, W. J. Hehre, J. S. Binkley, M. H. Gordon, D. J. Defrees, J. A. Pople, *J. Chem. Phys.* **1982**, *77*, 3654.

Received: October 23, 2006
Published Online: March 14, 2007

